Graz University of Technology
Institute of Applied Mechanics

Preprint Series

Preprint No 02/2013

Sound transmission through a poroelastic layered panel

Loris Nagler
Institute of Applied Mechanics, Graz University of Technology
Ping Rong
Departement of Acoustics and Vibrations, BMW Group
Martin Schanz
Institute of Applied Mechanics, Graz University of Technology
Otto von Estorff
Institute of Modelling and Computation, Hamburg University of Technology

Published in *Computational Mechanics*,
53(4), 549–560, 2014
The final publication is available at link.springer.com
DOI: 10.1007/s00466-013-0916-x

Abstract

Multi-layered panels are often used to improve the acoustics in cars, airplanes, rooms, etc. For such an application these panels include porous and/or fibrous layers. The proposed numerical method is an approach to simulate the acoustical behavior of such multi-layered panels.

The model assumes plate-like structures and, hence, combines plate theories for the different layers. The poroelastic layer is modelled with a recently developed plate theory. This theory uses a series expansion in thickness direction with subsequent analytical integration in this direction to reduce the three dimensions to two. The same idea is used to model either air gaps or fibrous layers. The latter are modeled as equivalent fluid and can be handled like an air gap, i.e., a kind of 'air plate' is used. The coupling of the layers is done by using the series expansion to express the continuity conditions on the surfaces of the plates. The final system is solved with finite elements, where domain decomposition techniques in combination with preconditioned iterative solvers are applied to solve the final system of equations.

In a large frequency range, the comparison with measurements shows very good agreement. From the numerical solution process it can be concluded that different preconditioners for the different layers are necessary. A reuse of the Krylov subspace of the iterative solvers pays if several excitations have to be computed but not that much in the loop over the frequencies.

1 Introduction

The acoustical design of buildings, aircrafts, cars, etc. has become a challenging task in engineering. It is especially of interest for automobile and aeronautical industry, since a good acoustical behavior not only improves the travel experiences of passenger, but also represents the quality of the product. Multi-layered panels are commonly used in these branches, as they can be very stiff and simultaneously light-weighted [11]. For the purpose of noise reduction, the panel can be reinforced by integrating layers made of fibrous or porous materials. For example, the fuselage of an aircraft usually contains an outer layer of aluminum, a noise insulation layer made of fibrous materials, and an inner layer, i.e., the cabin lining. In general, a multi-layered panel can be composed of a broad range of materials, which enables the panel to have rich acoustical and mechanical properties. However, this also brings up the question how to optimize the layers for a specific usage.

Measurements of the sound transmission loss of multi-layered panels are certainly one option and frequently used. The test facility consists of a reverberant room, an anechoic chamber, and a window between the two rooms holding the specimen. The specimen is excited by a diffuse sound field in the reverberant room and the transmitted sound energy is measured in the anechoic chamber, whose surfaces are covered with sound absorbing materials, such that the reflected waves cannot disturb the measurement. These measurements are usually time-consuming and expensive, especially when different combinations and configurations of material layers need to be tested for optimizing the design of a multi-layered setup.

To avoid measurements as much as possible simulation techniques have become more and more important. There are several numerical methods available (e.g., [2]), but it can be stated that the Finite Element Method (FEM) is mostly used also in an industrial environment. With a three-dimensional (3d) simulation different configurations can be tested before the first measurement is necessary. For the structural and acoustic part FE formulations are available [25, 13] and also for the porous noise insulating material [4, 15]. Hence, with the correct realisation of the coupling conditions they are ready to use. However, from structural mechanics it is well known that plate-like structures can be modelled more efficiently by special plate formulations. Not only the computing time is reduced, the meshing effort is in favor of plate or shell formulations as well.

For the above sketched multi-layered panel the outer skins can be modeled by well known formulations but the porous part and the air gap have to be considered differently. Based on Biot's theory of poroelasticity Nagler and Schanz [20] have proposed a plate theory and its corresponding FEM formulation. This formulation is based on a series expansion in thickness direction of the plate. Beside the porous layer, often such panels have also an air gap in between the different layers, which is mostly discretized by an expensive 3d FEM layer. This can be avoided by transferring the idea of the porous material, i.e., to apply a series expansion in thickness direction, to the air gap. This results in a 'air plate' as presented in [22]. In fact, a multi-layered panel can be simulated in a rather efficient way by a coupling of the different plate formulations. The surrounding air can be modelled in the standard way with a diffuse sound field and/or infinite elements.

To present such a numerical model and to validate it by measurements is the content of the paper at hand. The details of the poroelastic and the air plate theories can be found in [20] and [22], respectively. Hence, after recalling the essential steps of the poroelastic plate formulation, the special case of the elastic and the air plate are shown briefly. Next, the coupling conditions of different material combinations are discussed and the specialities for the different plate formulations are given. The final system of equations is not easy to be solved and, consequently, a strategy to use the structure of the system by a domain decomposition technique is presented. As well the efficient solution over a frequency range is studied. The essential part is the comparison of the numerical solution with a measurement. Besides, the numerical behavior of the solving process is reported.

In the following, all equations are stated in the frequency domain under the assumption that all quantities have a time-harmonic behavior (x_i being the spatial and t the time coordinate), i.e.,

$$\hat{f}(x_i,t) = f(x_i)e^{\mathrm{i}\omega t}$$

with the imaginary unit i and the angular frequency ω. Further, index-notation is used assuming an orthonormal Cartesian basis. Herein, a summation on repeated indices is imposed, a comma $()_{,i}$ denotes the spatial derivative and, as usual, the Kronecker delta is denoted by δ_{ij}. Throughout the paper, latin indices i,j,k take the values 1,2,3 and greek indices α,β the values 1,2.

2 Two-dimensional Layers

The geometry of any layer is considered to be plate-like, hence the extension in thickness direction x_3 is relatively small compared to its extension in the plane (x_1,x_2), i.e.,

$$\Omega = [(x_1,x_2,x_3) \in \mathbb{R}^3 \mid x_3 \in \left[-\frac{h}{2},\frac{h}{2}\right], (x_1,x_2) \in A \subset \mathbb{R}^2],$$

with x_i being the 3d spatial coordinates, h the thickness and A the middle surface. Such a layer is depicted in Fig. 1. In the following, the superscripts $()^e$ and $()^a$ will be used to distinguish between the *elastic* and the *acoustic* domains, respectively. The *poroelastic* domain will be denoted with $()^p$, however, at the solid displacement u_i and the pore pressure p the superscript is skipped.

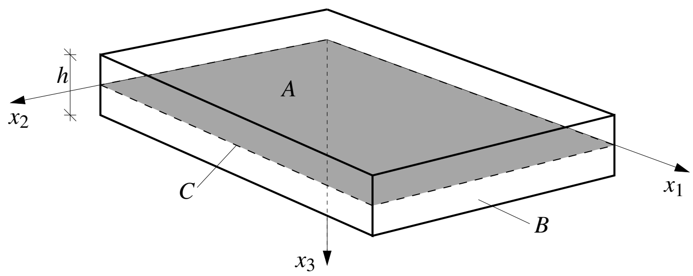

Figure 1: Geometry and coordinate system of a plate-like layer

2.1 Poroelastic Layer

Within a multi-layered system, the poroelastic layer represents the most complex one regarding its formulation. The main steps towards its reduction from 3d to 2d are outlined in this section, whereas details have been presented in [20].

The starting point is given by Biot's equations of poroelasticity [7, 8]. A poroelastic continuum consists of a solid skeleton and an interconnected fluid-filled pore system. Here, full saturation is assumed which allows the definition of the porosity as the ratio of the fluid volume to the overall volume $\phi = {}^{V^f}\!/_{V}$. A dynamic excitation of such a continuum causes the two phases to move relative to each other introducing friction and, thus, damping. Here, the so-called *u-p*–formulation is used. This means that the poroelastic continuum is completely expressed by the displacement field u_i of the solid skeleton and the pore pressure field p of the interstitial fluid. In index notation, the system of governing equations in frequency domain is

$$\mu u_{i,jj} + (\lambda+\mu)\, u_{j,ij} - (\alpha+\beta)\, p_{,i} + \omega^2(\rho+\beta\rho^f)\, u_i = -(f_i + \beta f_i^f) \tag{1a}$$

$$\frac{\beta}{\omega^2\rho_f}\, p_{,ii} - \frac{\phi^2}{R}\, p - (\alpha+\beta)\, u_{i,i} = \frac{\beta}{\omega^2\rho_f}\, f^f_{i,i}\,, \tag{1b}$$

where μ and λ are the Lamé parameters, α, β and R are poroelastic quantities, $\rho = (1-\phi)\rho^s - \phi\rho^f$ is the mean density of the continuum with ρ^s and ρ^f representing the densities of the solid and the fluid phases, respectively. Similarly, $f_i = (1-\phi) f_i^s - \phi f_i^f$ is the mean body force with f_i^s and f_i^f representing the respective body forces of the solid and the fluid phases.

The 3d equations (1) are transformed into a variational formulation. This is achieved by the usual procedure, namely a multiplication of both equations with the appropriate test-functions $\bar{u}_i$ and $\bar{p}$, respectively, and an integration over the considered domain Ω. A subsequent suitable integration by parts yields

$$\int\limits_{\Omega} \Bigg[\Big[\mu\,(u_{i,j} + u_{j,i}) + (\lambda u_{k,k} - \alpha\, p)\,\delta_{ij} \Big] \bar{u}_{i,j} + \Big[\beta \left(p_{,i} - f_i^f - \omega^2\rho^f u_i \right) - \left(f_i + \omega^2 \rho u_i \right) \Big] \bar{u}_i$$
$$- \frac{\beta}{\omega^2\rho^f} \Big[p_{,i} - \omega^2\rho^f u_i - f_i^f \Big] \bar{p}_{,i} - \Big[\alpha\, u_{k,k} + \frac{\phi^2}{R} p \Big] \bar{p} \Bigg] \mathrm{d}\Omega - \int\limits_{\Gamma_N} \Big[\sigma_{ij} n_j \bar{u}_i + \frac{1}{\mathrm{i}\omega} q_i n_i \bar{p} \Big] \mathrm{d}\Gamma_N = 0\,. \tag{2}$$

In the integral over the Neumann boundary Γ_N the quantity $\sigma_{ij}n_j$ represents the prescribed surface tractions (deduced from the total stress tensor [7]) and $q_i n_i$ the prescribed surface flux in normal direction. Due to the plate-like geometry, the domain integral in (2) can be split according to

$$\int\limits_{\Omega} (\cdot)\,\mathrm{d}\Omega = \int\limits_{A} \int\limits_{h} (\cdot)\,\mathrm{d}x_3\,\mathrm{d}A\,. \tag{3}$$

Similarly, the boundary integral can be split into an integral over the upper and the lower surfaces located at $x_3 = \pm{}^h\!/_2$ (represented by $A^\pm$) as well as an integral over the outer margin (see Fig. 1)

$$\int\limits_{\Gamma_N} (\cdot)\,\mathrm{d}\Gamma_N = \int\limits_{A^\pm} (\cdot)\,\mathrm{d}A^\pm + \int\limits_{C} \int\limits_{h} (\cdot)\,\mathrm{d}x_3\,\mathrm{d}C\,. \tag{4}$$

In order to evaluate the integrations over h, the primary variables u_i and p as well as the test-functions $\bar{u}_i$ and $\bar{p}$ are replaced by power series in thickness direction

$$\begin{aligned} u_i(x_1,x_2,x_3) &= \sum_{k=0}^{\infty} \overset{k}{u}_i(x_1,x_2)x_3^k \\ p(x_1,x_2,x_3) &= \sum_{k=0}^{\infty} \overset{k}{p}(x_1,x_2)x_3^k , \end{aligned} \tag{5a}$$

$$\begin{aligned} \bar{u}_i(x_1,x_2,x_3) &= \sum_{\ell=0}^{\infty} \overset{\ell}{\bar{u}}_i(x_1,x_2)x_3^\ell \\ \bar{p}(x_1,x_2,x_3) &= \sum_{\ell=0}^{\infty} \overset{\ell}{\bar{p}}(x_1,x_2)x_3^\ell . \end{aligned} \tag{5b}$$

In (5), it can be observed that the unknown dependency on x_3 is approximated by a polynomial. On the other hand, new unknown quantities of the order k and ℓ are introduced which, however, only depend on the two in-plane coordinates x_1 and x_2. With (5) in (2) and with the integrals split according to (3) and (4), the integration over the thickness can be analytically evaluated, leaving an expression which is entirely defined on the domain A, i.e., the middle surface, and its boundary curve C. A detailed derivation of the two-dimensional poroelastic equations can be found in [20] and [19]. However, a few interesting aspects shall be pointed out.

A remarkable observation is the decoupling of the out-of-plane (plate) and the in-plane (disc) formulation, i.e., the two problems can be solved independently of each other. In linear elasticity, only the plate formulation would be considered any further as long as the load acts perpendicular to the middle surface of the structure. In the poroelastic case, however, this simplification was shown to be not appropriate. Indeed, it turns out that the solution of the pore pressure field crucially depends on whether the load is applied on one surface only or is split in two parts one acting on the upper and the other on the lower surface. Hence, for obtaining the overall solution both the out-of-plane and the in-plane formulation need to be considered. Moreover, when coupling several layers, the neutral axis with respect to pure bending does not coincide with the middle surfaces of the individual layers. This makes it necessary to consider the disc problem in each layer even for the elastic case.

Before starting any calculations, the power series (5) need to be truncated. It turns out that only very few coefficients are required to adequately model even relatively thick structures. Indeed, if considering all quantities up to $k = \ell = 3$, various effects are considered such as the thickening of one half and the thinning of the other half during bending, a change in thickness due to a stretching as well as a warping of the cross section. The truncation allows great flexibility. Indeed any quantity can be approximated by an individual amount of coefficients, e.g., the vertical displacement may be approximated up to the second order, while the in-plane displacement is considered only linearly and the pore pressure up to the cubic term.

2.2 Elastic Layer

The procedure for obtaining a two-dimensional formulation for an elastic layer coincides with the one for the poroelastic layer, except that it is less cumbersome, since it only features the displacement field u_i^e. The governing equation may be obtained by setting $\phi = \alpha = \beta = 0$ in (1a) and neglecting (1b)

$$\mu u^e_{i,jj} + (\lambda + \mu)\, u^e_{j,ij} + \omega^2 \rho\, u^e_i = -f_i\,. \tag{6}$$

The variational formulation is a simplified version of (2), namely

$$\int\limits_{\Omega^e} \left[\left[\mu \left(u^e_{i,j} + u^e_{j,i} \right) + \lambda\, u^e_{k,k} \delta_{ij} \right] \bar{u}^e_{i,j} - \left[f_i + \omega^2 \rho u^e_i \right] \bar{u}^e_i \right] \mathrm{d}\Omega^e - \int\limits_{\Gamma^e_N} \sigma^e_{ij} n^e_j \bar{u}^e_i \,\mathrm{d}\Gamma^e_N = 0\,. \tag{7}$$

Above, $\sigma^e_{ij} n^e_j$ again represents the prescribed surface tractions, this time however, deduced from the solid stress tensor.

The unknown field quantity and the test-function are replaced by power series in thickness direction

$$\begin{aligned} u^e_i(x_1,x_2,x_3) &= \sum_{k=0}^{\infty} \overset{k}{u}{}^e_i(x_1,x_2) x_3^k \\ \bar{u}^e_i(x_1,x_2,x_3) &= \sum_{\ell=0}^{\infty} \overset{\ell}{\bar{u}}{}^e_i(x_1,x_2) x_3^\ell\,. \end{aligned} \tag{8}$$

The uncoupling of the disc and the plate formulations is again observed. As mentioned earlier, when considering a single elastic layer under vertical load, the disc problem could be omitted (still, a small error is introduced). However, when combining several layers, the neutral bending-axis is shifted from the individual middle surfaces and both formulations are required for obtaining the overall solution.

In [19], the elastic plate-equations have been analyzed regarding the needed amount of coefficients for obtaining a suitable model. Therein, it is shown that including the coefficients $\overset{0}{u}{}^e_3$, $\overset{2}{u}{}^e_3$ and $\overset{1}{u}{}^e_\alpha$ (with $\alpha = 1,2$) leads to a plate equation settling somewhere between the Kirchhoff and the Mindlin model. Including additionally $\overset{3}{u}{}^e_\alpha$, an 'enhanced' Mindlin model is deduced. It should be remarked that the above sketched plate formulation is very similar to the work of Kienzler [16, 17].

2.3 Air Layer

Since the multi-layered panel may include some air layer between any two poroelastic and/or elastic layers, it may be reasonable to model it two-dimensionally as well. The equation governing wave propagation in a homogeneous and compressible fluid is the wave equation. In the frequency domain, it is transformed to the Helmholtz equation

$$p^a_{,ii} + \frac{\omega^2}{c^2} p^a = 0\,, \tag{9}$$

with p^a being the acoustic pressure and c the wave speed. The respective variational formulation is again deduced by the standard procedure. In view of the coupling, the variational form is additionally multiplied by $-1/\omega^2\rho^a$ for convenience. This leads to

$$\int\limits_{\Omega^a} \left[\frac{1}{\omega^2 \rho^a} p^a_{,i} \bar{p}^a_{,i} - \frac{1}{c^2 \rho^a} p^a \bar{p}^a \right] \mathrm{d}\Omega^a - \int\limits_{\Gamma^a_N} \frac{1}{\omega^2 \rho^a} p^a_{,i} n^a_i \bar{p}^a \,\mathrm{d}\Gamma^a_N = 0\,. \tag{10}$$

The acoustic pressure and its test-function are once again replaced by the power series

$$
\begin{aligned}
p^a(x_1,x_2,x_3) &= \sum_{k=0}^{\infty} \overset{k}{p}{}^a(x_1,x_2)x_3^k \\
\bar{p}^a(x_1,x_2,x_3) &= \sum_{\ell=0}^{\infty} \overset{\ell}{\bar{p}}{}^a(x_1,x_2)x_3^\ell \,.
\end{aligned}
\tag{11}
$$

Again, a decoupling occurs, this time extra simple, since the field under consideration is scalar. The quantity $p^a_{,i}n^a_i$ on Γ^a_N represents the prescribed pressure gradient, i.e., the fluid flux in normal direction. Details of this formulation of an 'air plate' and a validation can be found in [22].

3 Coupling of layers and surrounding fluid

With the poroelastic layer, the elastic layer, and the air layer a complete panel can be assembled. In order to couple the layers among each other over their surfaces, suitable coupling conditions have to be formulated for guaranteeing equilibrium of stresses, continuity of displacements and equilibrium of pressure at the interfaces. The coupling between three-dimensional poroelastic, elastic and acoustic continua has been presented in [4]. The coupling conditions on the acoustic-poroelastic interface are

$$
\begin{aligned}
u^a_i n^a_i &= -u^p_i n^p_i \\
p^a \delta_{ij} n^a_j &= \sigma_{ij} n^p_j \\
p^a &= p \,.
\end{aligned}
\tag{12}
$$

On the acoustic-elastic interface, it is

$$
\begin{aligned}
u^a_i n^a_i &= -u^e_i n^e_i \\
p^a \delta_{ij} n^a_j &= \sigma^e_{ij} n^e_j \,.
\end{aligned}
\tag{13}
$$

Since the acoustic fluid is expressed by means of the sound pressure p^a rather than the particle displacement u^a_i, this latter quantity is replaced by $u^a_i = {}^1\!/\!_{\omega^2\rho^a}\, p^a_{,i}$. The field u^p_i is defined as the mean displacement of a 'poroelastic particle', similarly as the mean density in (1), namely $u^p_i = (1-\phi)u_i + \phi u^f_i = u_i + {}^1\!/\!_{\mathrm{i}\omega} q_i$, with $q_i = \mathrm{i}\omega\phi(u^f_i - u_i)$ being the flux of the pore-fluid. Note that the displacement conditions only enforce continuity in the normal direction since the fluid cannot prevent relative displacements in tangential direction. Finally, on the elastic-poroelastic interface one needs to fulfill the conditions

$$
\begin{aligned}
u^e_i &= u^p_i \\
\sigma^e_{ij} n^e_j &= \sigma_{ij} n^p_j \\
q_i n^p_i &= 0 \,.
\end{aligned}
\tag{14}
$$

This time, the displacements need to be continuous in the tangential direction as well. Due to the impermeable elastic layer, no fluid flux appears on the interface.

The coupling integrals may now be deduced by combining the boundary integrals of the variational formulations (2), (7) and (10). Indeed, the parts of the integrals living on the same interface occupy the very same surface in physical space. For example, on the acoustic-poroelastic interface, this yields

$$I^{ap} = -\int\limits_{\Gamma^{ap}} \left[\frac{1}{\omega^2 \rho^a} p^a_{,i} n^a_i \bar{p}^a + \sigma_{ij} n^p_j \bar{u}_i + \frac{1}{\mathrm{i}\omega} q_i n^p_i \bar{p} \right] \mathrm{d}\Gamma^{ap} . \tag{15}$$

By incorporating the conditions (12) into (15) under consideration of the above mentioned replacements for u^a_i and u^p_i, one obtains

$$I^{ap} = -\int\limits_{\Gamma^{ap}} \left[p^a \bar{u}_i n^a_i - u_i n^p_i \bar{p}^a \right] \mathrm{d}\Gamma^{ap} . \tag{16}$$

The expression above covers the Neumann-type interface conditions, whereas the continuity of the pressure (Dirichlet-type condition) has to be additionally enforced as it will be explained at the end of this section. The acoustic-elastic interface is governed by the very similar expression

$$I^{ae} = -\int\limits_{\Gamma^{ae}} \left[p^a \bar{u}^e_i n^a_i - u^e_i n^e_i \bar{p}^a \right] \mathrm{d}\Gamma^{ae} . \tag{17}$$

The elastic-poroelastic interface gives

$$I^{ep} = 0 \tag{18}$$

and the coupling between these two layers is therefore natural. Only the Dirichlet-type interface conditions, namely the continuity of displacements, has to be additionally enforced.

The conditions for coupling two-dimensional structures are obviously the same as for coupling three-dimensional ones. In the former case, however, it must be accounted for the fact that the interfaces are located at a certain distance from the middle surface of the layers while all quantities incorporated into the formulation are solely defined on the middle surface itself. Moreover, as pictured in Fig. 2, each layer has its own coordinate system with origin on its middle surface. This requires to replace the unknown quantities by the corresponding power series evaluated at the respective location of each local coordinate system. For the acoustic-poroelastic interface the power series take the form

$$u_i = \sum_{k=0}^{\infty} \overset{k}{u}_i \left(\frac{h^p}{2} \right)^k \qquad p^a = \sum_{k=0}^{\infty} \overset{k}{p} \left(-\frac{h^a}{2} \right)^k \tag{19a}$$

$$\bar{u}_i = \sum_{\ell=0}^{\infty} \overset{\ell}{\bar{u}}_i \left(\frac{h^p}{2} \right)^k \qquad \bar{p}^a = \sum_{\ell=0}^{\infty} \overset{\ell}{\bar{p}} \left(-\frac{h^a}{2} \right)^k . \tag{19b}$$

As it can be seen from Fig. 2, the normal vectors at the interface are $n^a_i \mathbf{e}_i = [0,0,1]^\top$ and $n^p_i \mathbf{e}_i = [0,0,-1]^\top$. Using this, together with the expressions (19) in (16), the coupling integral for the

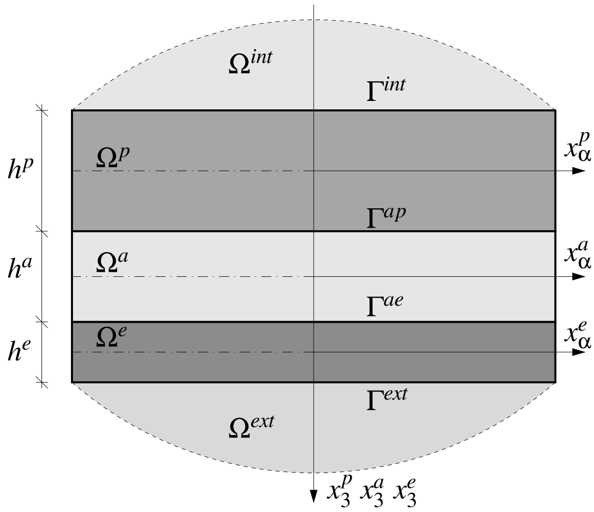

Figure 2: Coupled system consisting of two acoustic domains separated by a multi-layered structure. The structure features a poroelastic, an acoustic and an elastic layer. Each layer has its own local coordinate systems.

two-dimensional layers becomes

$$
\begin{aligned}
I^{ap} = \sum_{\ell=0}^{\infty}\sum_{k=0}^{\infty} \int_{\Gamma^{ap}} \Bigg[&\left(\frac{h^p}{2}\right)^{\ell} \left(-\frac{h^a}{2}\right)^{k} \overset{k}{p}{}^{a}\, \overset{\ell}{\bar{u}}_3 \\
&+ \left(-\frac{h^a}{2}\right)^{\ell} \left(\frac{h^p}{2}\right)^{k} \overset{k}{u}_3\, \overset{\ell}{\bar{p}}{}^{a} \Bigg] \mathrm{d}\Gamma^{ap} .
\end{aligned} \tag{20}
$$

The very same considerations apply on the acoustic-elastic interface of Fig. 2. Of course, this time, the acoustic pressure p^a is evaluated at $h^a/2$, whereas the elastic displacement field u_i^e is evaluated at $-h^e/2$. This yields

$$
I^{ae} = -\sum_{\ell=0}^{\infty}\sum_{k=0}^{\infty} \int_{\Gamma^{ae}} \left[\left(-\frac{h^e}{2}\right)^{\ell} \left(\frac{h^a}{2}\right)^{k} \overset{k}{p}{}^{a}\, \overset{\ell}{\bar{u}}{}^{e}_3 + \left(\frac{h^a}{2}\right)^{\ell} \left(-\frac{h^e}{2}\right)^{k} \overset{k}{u}{}^{e}_3\, \overset{\ell}{\bar{p}}{}^{a} \right] \mathrm{d}\Gamma^{ae} . \tag{21}
$$

An elastic-poroelastic interface does not appear in Fig. 2. Even if it did, the respective coupling integral (18) would be *zero* anyway. In view of a finite element discretization, each expression resulting from any combination of k and ℓ in the double sums of (20) and (21), represents coupling matrices located at specific off-diagonal positions in the overall system matrix.

The coupling of the outermost layers with the adjacent three-dimensional acoustic fluid domains Ω^{int} and Ω^{ext} follows the exact same pattern as presented above, with the only difference that the displacement fields in (16) or (17) are replaced by the respective power series.

The last point to be discussed in this section regards the imposition of the Dirichlet-type interface conditions. As already mentioned, the two-dimensional formulation only provides degrees of freedom on the middle surface, whereas the coupling needs to be imposed at the interface. This means that once again, the power series evaluated at the respective interface need to be used. The condition itself is imposed by means of Lagrangian multipliers. For example, the condition enforcing equilibrium of pressure $p - p^a = 0$ at Γ^{ap} in Fig. 2 is stated in the form

$$\Pi^{ap} = \int_{\Gamma^{ap}} \upsilon(p - p^a)\,\mathrm{d}\Gamma^{ap}\,, \tag{22}$$

with υ being the Lagrangian multiplier. The first variation of (22) is given by

$$\delta\Pi^{ap} = \int_{\Gamma^{ap}} [(p\,\bar{\upsilon} + \upsilon\,\bar{p}) - (p^a\,\bar{\upsilon} + \upsilon\,\bar{p}^a)]\,\mathrm{d}\Gamma^{ap}\,. \tag{23}$$

Inserting the power series for p and p^a evaluated at the interface yields

$$\delta\Pi^{ap} = \sum_{k=0}^{\infty}\left(\frac{h^p}{2}\right)^k \int_{\Gamma^{ap}} \left[(\overset{k}{p}\,\bar{\upsilon} + \upsilon\,\overset{k}{\bar{p}})\right]\mathrm{d}\Gamma^{ap} - \sum_{k=0}^{\infty}\left(-\frac{h^a}{2}\right)^k \int_{\Gamma^{ap}} \left[(\overset{k}{p}{}^a\,\bar{\upsilon} + \upsilon\,\overset{k}{\bar{p}}{}^a)\right]\mathrm{d}\Gamma^{ap}\,. \tag{24}$$

Similarly, the continuity of displacements $u_i - u_i^e = 0$ on an elastic-poroelastic interface Γ^{ep} (not appearing in Fig. 2) is enforced by

$$\delta\Pi^{ep} = \sum_{k=0}^{\infty}\left(-\frac{h^p}{2}\right)^k \int_{\Gamma^{ep}} \left[(\overset{k}{u}_i\,\bar{\upsilon}_i + \upsilon_i\,\overset{k}{\bar{u}}_i)\right]\mathrm{d}\Gamma^{ep} - \sum_{k=0}^{\infty}\left(\frac{h^e}{2}\right)^k \int_{\Gamma^{ep}} \left[(\overset{k}{u}{}_i^e\,\bar{\upsilon}_i + \upsilon_i\,\overset{k}{\bar{u}}{}_i^e)\right]\mathrm{d}\Gamma^{ep}\,. \tag{25}$$

On the acoustic-elastic interface, no Dirichlet-type interface conditions need to be imposed.

In a Finite Element formulation for each order k off-diagonal coupling matrices are obtained which are assembled into the overall system matrix. Therewith, all required expressions have been presented for coupling any of the presented layers among each other.

4 Numerical realisation

In the previous sections, the variational principles for the layers as well as for the coupling conditions have been provided. The FEM realisation is done by means of standard elements and does not need to be discussed here. However, for realistic systems it is a difficult task to solve the equation system. Further, for various mechano-acoustical applications, like the prediction of sound transmission through multi-layered panels, often the response not only for one frequency but for a frequency range has to be determined. This means that for each frequency step a whole system has to be solved. If the difference between two frequencies is small, their assembled system matrices are usually rather similar. This property might be used in combination with an iterative equation solver.

An iterative solution process can be accelerated by using the subspace recycling method *GCRO-DR*. In general, *GCRO-DR* is an iterative projection solver based on Krylov subspaces [21]. It is composed of an inner solver *GMRES*, with deflated restarting (*GMRES-DR*), and an outer solver *GCR* with an orthogonalization (*GCRO*) [9]. The algorithm starts solving the first system of equations with the inner solver. Following the general solving scheme of the iterative projection method, *GMRES-DR* attempts to minimize the residual. When the solver converges, it also

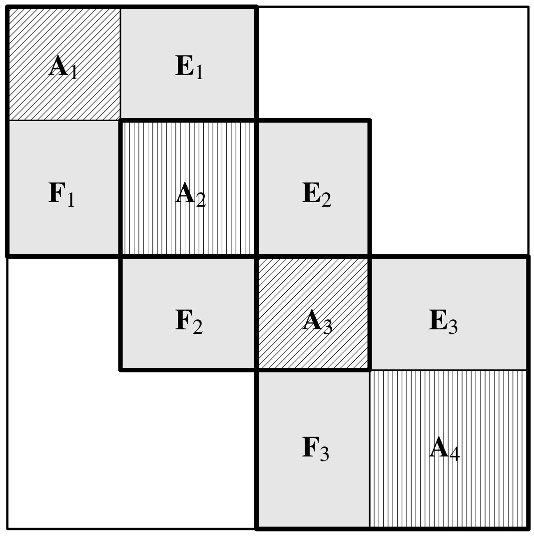

Figure 3: Sparse pattern of a finite element model of the multi-layered panel.

generates a solution subspace which contains the information about the approximated solution. The *GCRO-DR* extracts a set of harmonic Ritz vectors that provide an optimal approximation of the most representative interior eigenvectors of the solution subspace and passes it to the outer solver *GCRO*. This set of harmonic Ritz vectors is orthogonalized by *GCRO*, such that a recycling subspace is generated. In other words, the recycling subspace preserves the most important part of the solution subspace and can be reused by the inner solver for a new system of equations. As mentioned above, system matrices are rather similar for adjacent frequencies. It can be assumed that these systems can be solved on a similar solution subspace as well. Therefore, the solution process can be accelerated with the help of the obtained recycling subspace. In practice, *GCRO-DR* has been treated as a multi-frequency solver for acoustical problems in [6]. In this work, it is used for the sound transmission problem of the multi-layered panel.

As one of the Krylov subspace methods, *GCRO-DR* suffers from the common convergence problem when a system matrix is badly conditioned. Especially, the sound transmission problem of a multi-layered panel can consist of different material models, where the formulation of the Helmholtz equation in an acoustical domain leads to an indefinite system matrix. Moreover, the system matrix of the poroelastic plate is often ill-conditioned [3, 13, 20]. Therefore, for applying *GCRO-DR* successfully a suitable preconditioner is essential. In the preconditioning strategy a rather helpful characteristic of a multi-layered panel problem should be taken into account: The layers of a panel are coupled subsequently, thus, the resulting system matrix usually reveals a special sparse pattern as shown in Fig. 3, where sub-matrix $\mathbf{A}_i$ represent the system matrix of each layer, and $\mathbf{E}_i$ and $\mathbf{F}_i$ the respective coupling matrices. It can be seen that each sub-matrix is only coupled with its direct neighbors. Therefore, any adjacent two sub-matrices $\mathbf{A}_i$ and $\mathbf{A}_{i+1}$

and their respective coupling matrices $\mathbf{E}_i$ and $\mathbf{F}_i$ form a 2 by 2 block matrix. Because of this nature of the system matrix, a preconditioning algorithm based on the hybrid (direct/iterative) solver HIPS (Hierarchical Iterative Parallel Solver) [12] and the ARMS (Algebraic Multilevel Solver) [23] is used in this work. Both, HIPS and ARMS are domain decomposition solvers based on the Schur complement. The original ARMS utilizes a graph partitioning method to sort the system matrix into a 2 by 2 block form, which is not necessary in the actual application (see the structure in Fig. 3). Such a 2 by 2 block system can be factorized by using the Schur complement [12]

$$\begin{bmatrix}\mathbf{B} & \mathbf{E}\\ \mathbf{F} & \mathbf{C}\end{bmatrix} \approx \begin{bmatrix}\mathbf{L}_B & 0\\ \mathbf{F}\mathbf{U}_B^{-1} & \mathbf{L}_C\end{bmatrix} \times \begin{bmatrix}\mathbf{U}_B & \mathbf{L}_B^{-1}\mathbf{E}\\ 0 & \mathbf{U}_C\end{bmatrix}. \tag{26}$$

Usually, the upper left sub-matrix $\mathbf{B}$ has a rather small size, such that it can be easily decomposed into a pair of upper und lower triangular matrices $\mathbf{U}_B$ and $\mathbf{L}_B$ by incomplete factorization (ILU). While the lower right sub-matrix $\mathbf{C}$ still contains a large number of degrees of freedom, its respective triangular matrices $\mathbf{U}_C$ and $\mathbf{L}_C$ can be obtained by appling the same algorithm recursively. HIPS can be regarded as an extension of ARMS. It uses both ILU and complete factorization (LU) to factorize the sub-matrix $\mathbf{B}$. In general, LU can provide more stability to the solving process but it is more expensive than ILU. However, the method still performs well as long as the size of $\mathbf{B}$ is limited. As aforementioned, the multi-layered panel problem is structured in a series of 2×2 blocks due to its geometrical property. Therefore, the Schur complement method can be directly used to factorize the system matrix. Furthermore, the factorization process can be simplified. Since the material layers are only coupled to its direct neighbours, each 2×2 block can be factorized independently following (26), such that

$$\begin{bmatrix}\mathbf{A}_i & \mathbf{E}_i\\ \mathbf{F}_i & \mathbf{A}_{i+1}\end{bmatrix} \approx \begin{bmatrix}\mathbf{L}_i & 0\\ \mathbf{F}_i\mathbf{U}_i^{-1} & \mathbf{L}_{i+1}\end{bmatrix} \times \begin{bmatrix}\mathbf{U}_i & \mathbf{L}_i^{-1}\mathbf{E}_i\\ 0 & \mathbf{U}_{i+1}\end{bmatrix}. \tag{27}$$

It should be noted that each sub-matrix $\mathbf{A}_i$ or $\mathbf{A}_{i+1}$ needs to be factorized only once. In the subsequent 2×2 block, the current lower right sub-matrix $\mathbf{A}_{i+1}$ is shifted to the upper left block and the lower right block is occupied by the new sub-matrix $\mathbf{A}_{i+2}$. This means that the LU/ILU decomposition of $\mathbf{A}_{i+1}$ can be reused to factorize the new 2×2 block.

The most challenging part of solving a multi-layered system is that it contains different finite element formulations. By using the domain decomposition method, fortunately, the material models can be preconditioned separately. Under some conditions (see section 5), the subspace recycling method *GCRO-DR* solves effectively the problem over a frequency range.

All FE models are implemented by using the finite element library *libMesh* [18] and the linear solver package *PETSc* [5]. The calculations are executed on a computer with Intel® Core™2 Quad Processor Q9650 and 8GB RAM.

5 Example: Five-layer panel

In this example, the transmission loss of a five-layer panel, which includes all the described plate models, is calculated and validated by measurement. The setup of the panel is shown in Fig. 4.

The first layer is a 2 mm aluminum plate where a 2.5 cm fibrous blanket is placed on top. This fibrous blanket is shown in Fig. 5 and can be regarded as a specific acoustic fluid (see [1]) in

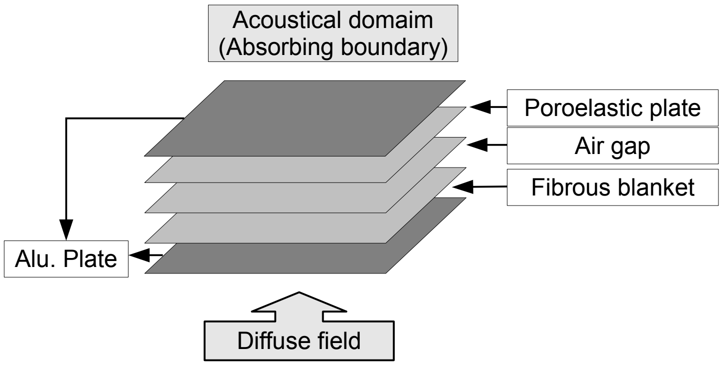

Figure 4: A pictorial view of the five-layer panel.

Figure 5: Photo of the Microlite® AA fibrous blanket

the simulation. The respective experimental setup of this part of the panel is shown in Fig. 6. The fibrous blanket is constrained by a metal net, such that its thickness is somewhat controlled. Next, a 2.5 cm thick wooden frame is mounted in the open window, in this way, an air gap is created between the fibrous blanket and the upcoming layers. Subsequent to the air gap, a poroelastic layer (plate) is placed on the wooden frame. Finally, the other 2 mm aluminum plate is placed on the poroelastic plate. A photo of the poroelastic plate and the cover plate is shown in Fig. 7. The used material parameters can be found in Tab. 1, Tab. 2, and Tab. 3.

All the layers are discretized by 30×30 *QUAD4* elements and the acoustical domain by 5 layers of 30×30 *HEX8* elements. The infinite extension of the acoustic domain is modelled with infinite elements as proposed in [10]. The first aluminum plate is modeled with the formu-

Table 1: Acoustical properties of air and the material properties of the aluminum plate.

Acoustics in air		Aluminum plate		
Speed of sound	Density	Young's modulus (E)	Density	Poisson's ratio
$343.3\,\mathrm{m/s}$	$1.21\,\mathrm{kg/m^3}$	$7.1 \cdot 10^{10}\,\mathrm{N/m^2}$	$2700\,\mathrm{kg/m^3}$	0.33

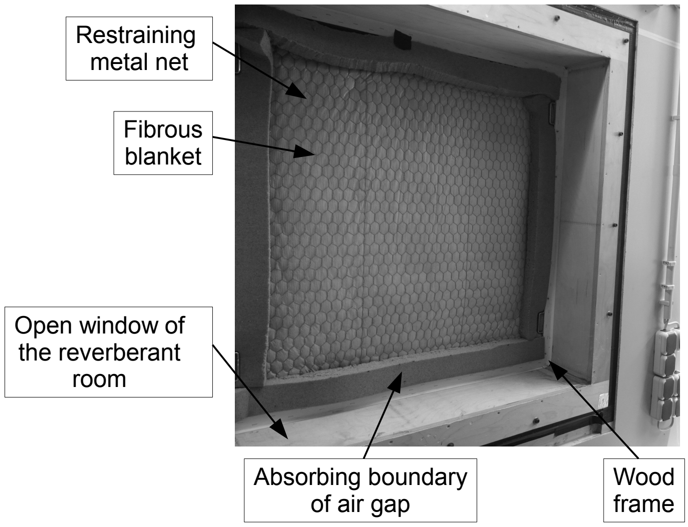

Figure 6: A pictorial view of the experimental setup of the five-layer panel (the aluminum plate on the excitation side, the fibrous blanket, and the air gap).

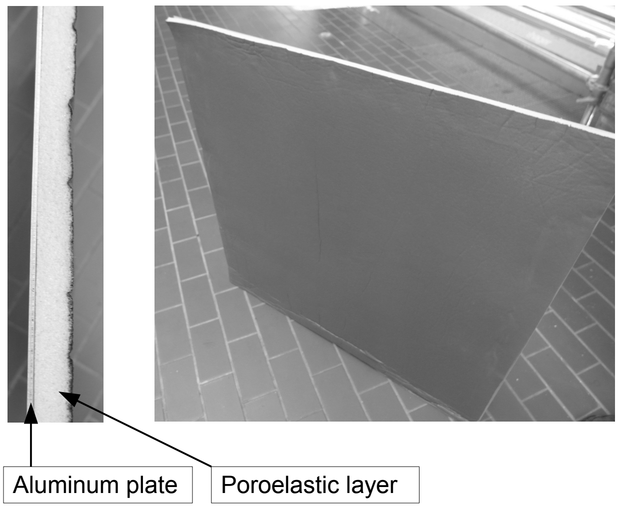

Figure 7: A pictorial view of the experiment setup of the five-layer panel (the poroelastic layer and the cover aluminum plate).

Table 2: Material properties of the Microlite® AA fibrous blanket as specific acoustical fluid. The data is referred to [24].

Speed of sound	Density
$120\,{}^{\mathrm{m}}/_{\mathrm{s}}$	$7\,{}^{\mathrm{kg}}/_{\mathrm{m}^3}$

Table 3: Material properties of the poroelastic layer.

Density	Poisson ratio	Young's modulus	Porosity	Fluid resistance
$5.6\,\mathrm{kg/m^3}$	0.43	$1.28 \cdot 10^4\,\mathrm{N/m^2}$	0.995	$4.63 \cdot 10^4\,\mathrm{Ns/m^4}$

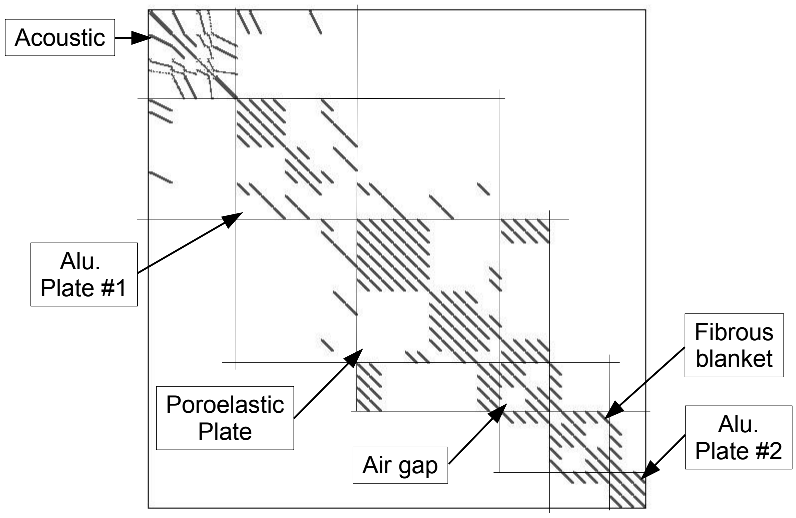

Figure 8: The matrix sparsity pattern of the five-layer model. The aluminum plate No.1 is formulated by the poroelastic plate model, with the *DOFs* of pore pressure being eliminated, the air gap and the fibrous blanket are formulated by the acoustic plate model, and the aluminum plate No.2 by the Mindlin plate formulation.

lation. The acoustic plate model is used for the fibrous blanket and the air gap. For the fibrous blanket complex material data are used as suggested in [1]. The poroelastic layer is computed with the poroelastic plate model. It should be noted that both the poroelastic plate formulation and the poroelastic disc formulation, as described in section 2, are included in the model. For testing purposes, the cover aluminum plate is formulated by the poroelastic model as well, as proposed by Nagler [19], where the model is modified by simply eliminating the *DOFs* of the pore pressure. In this way, the in-plane (disc) motion of the plate is also considered. Moreover, third order approximations are used for all the poroelastic plate models and the acoustic plate model. This yields a linear system with 41562 *DOFs*, whose sparsity pattern is shown in Fig. 8.

The condition number of the linear system has a magnitude of order 10^{41}. As discussed in section 4, each layer is separated into an individual sub-domain and can be factorized with a different method. For the acoustic plate models and the acoustical domain, an *ILU* preconditioner with a drop threshold of $\tau = 10^{-3}$ is used. The Mindlin plate is preconditioned with an

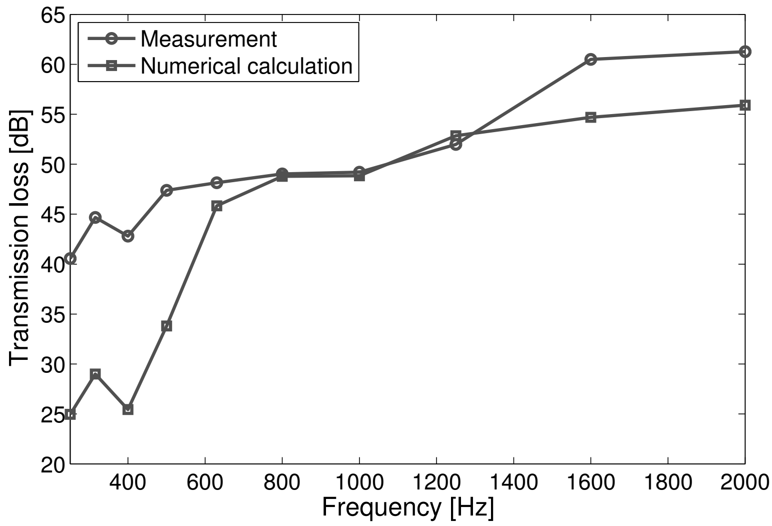

Figure 9: Validation of the transmission loss calculation of the five-layer panel, which is composed of two aluminum outer plates, a poroelastic layer, an air gap, and a fibrous blanket in between.

ILU with 1 fill-in level. Unfortunately, none of the incomplete factorizations seems to work with the poroelastic plate models. In order to obtain the preconditioner for further calculations, the respective sub-matrices are directly factorized by *LU*.

GMRES is used to solve the transmission loss problem first. The predicted results are compared with the measurement in Fig. 9. It can be seen that the calculation shows a perfect agreement in the frequency range from 600 to 1400 Hz. Above 1400 Hz, the calculated results are about 5 dB smaller than the measurement. Except for the fact that the ISO-measurement typically has a 3 dB error margin [14], the setup of the multi-layered panel is relatively complicated. Therefore, the 5 dB difference can be still considered as a good agreement. However, the calculation and the measurement differ significantly below 500 Hz. This can be caused partially by the measurement, since the diffuse field generated in the reverberant room may have a rather poor quality in the frequency range close to the Schroeder frequency (in this case 290 Hz). In fact, the same effect can be observed in other examples. The required iteration steps and computational time of *GMRES* are shown in Fig. 10 and 11. It can be seen that *GMRES* converges at about 900 iterations and it takes about 30 minutes for each frequency.

Furthermore, *GCRO-DR* is applied to solve the current example. Since the solution subspace generated by *GMRES* has the size of about 900, a recycling subspace with 100 vectors is tested first. The preconditioner is updated every 30 Hz. However, the solver stagnates after several frequency steps. In order to make it work, the size of the recycling subspace cannot be set larger than 30, which is only about 3% of the solution subspace. With the size of the recycling subspace being 30, the iteration number and the respective computational time required by *GCRO-DR* are shown in Fig. 12 and 13.

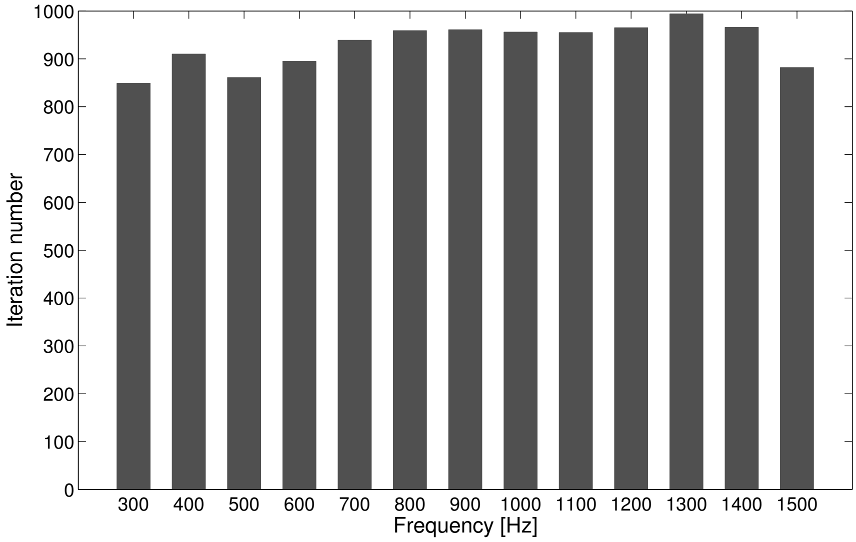

Figure 10: The iteration number required by *GMRES* for solving the transmission loss of the five-layer panel.

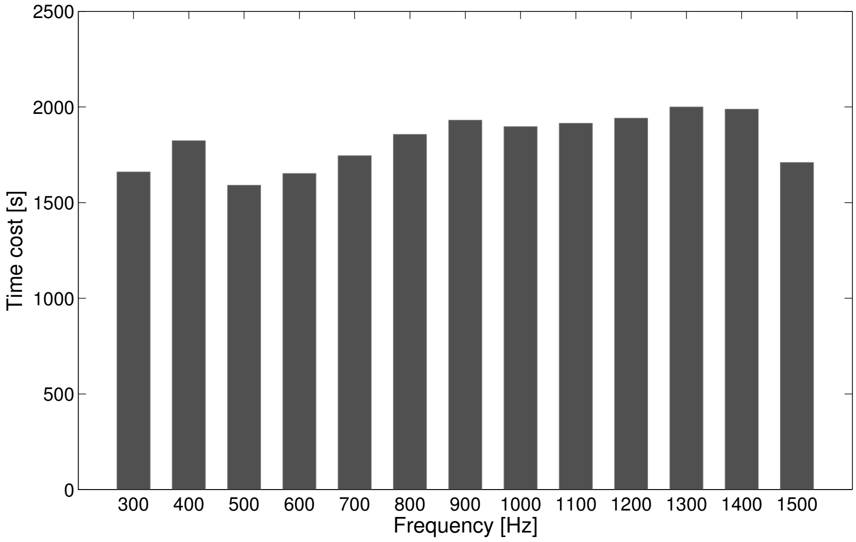

Figure 11: The computational time required by *GMRES* for solving the transmission loss of the five-layer panel.

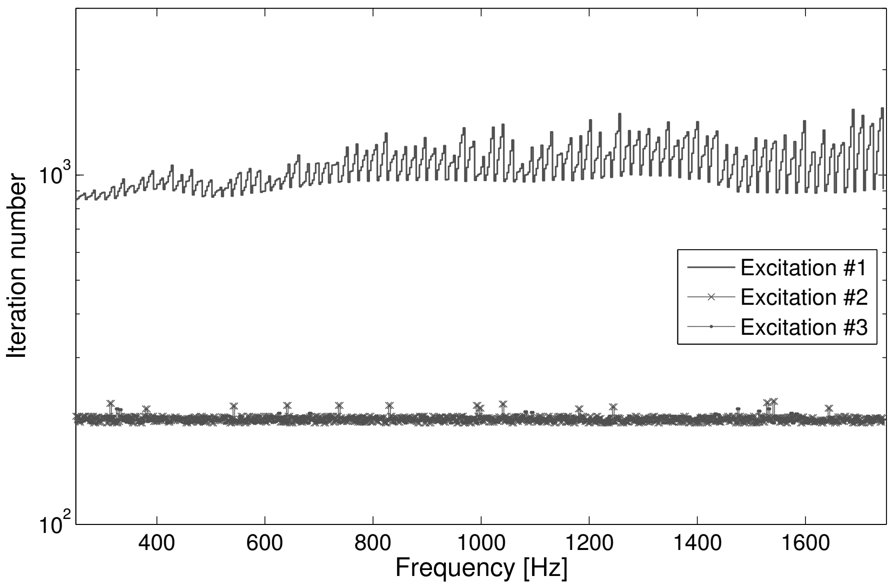

Figure 12: The iteration number required by *GCRO-DR* for solving the first three excitations of the five-layer panel problem at 5 Hz resolution.

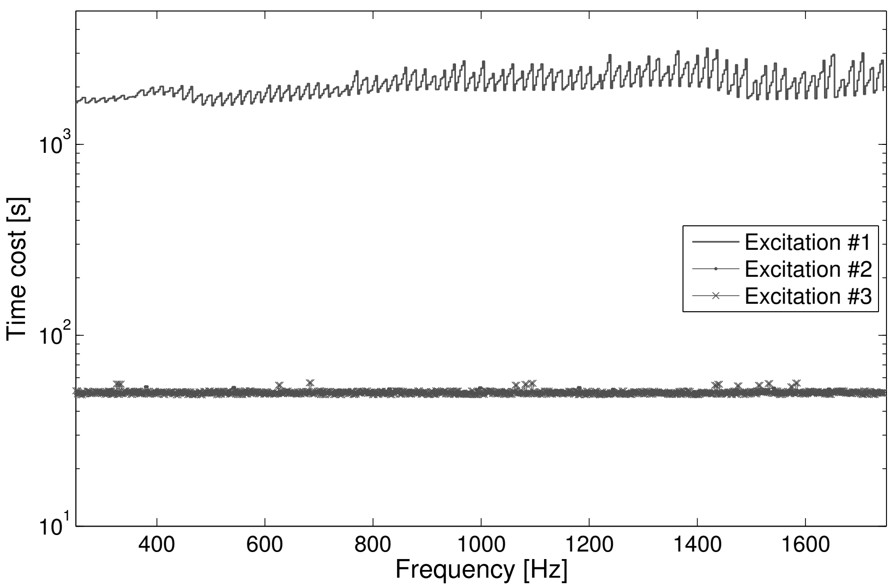

Figure 13: The computational time required by *GCRO-DR* for solving the first three excitations of the five-layer panel problem at 5 Hz resolution.

6 Conclusions

Based on Biot's theory of poroelasticity a plate formulation to describe the acoustical behavior of plate-like structures has been discussed. The dimension reduction from 3d to 2d is performed with a series expansion in thickness direction and a subsequent analytical integration. The same technique can be applied to elastic plates resulting in similar theories like Reissner and Mindlin. Not only structural elements can be formulated in such a way but also a 'air plate' has been constructed to ease the formulation of air gaps in multi-layered panels. The coupling between different layers, i.e., different materials, is similar to the 3d case but the degrees of freedom from the mid plane have to be transfered to the surface of each panel by using the series expansion.

The overall system is discretized with standard finite elements. However, the final system of equations is large in the case of higher frequencies and not well conditioned. But taking the structure of the geometry and the different domains via a domain decomposition into account, different preconditioners for each domain can be used and a nested iterative solution procedure can be applied.

The final model has been validated by an experimental setup for measuring the transmission loss factor. Over a large frequency range the agreement between the measurement and the computation is very good. Only for small frequencies larger differences can be observed. However, in this range the measuring setup may not produce a diffusive sound field and, hence, the numerical results cannot match. Further, the numerical behavior of the iterative solver and the preconditioner has been studied. It can be concluded that ILU based preconditioners are sufficient if each layer is handled by its own. The only exception is the poroelastic plate where a working preconditioner is an open question. Further, a recycling of the subspaces of the Krylov solver is advantageous if the same problem is computed for several excitations.

Acknowledgement The authors gratefully acknowledge the financial support by a common project of the Austrian Science Fund (FWF, grant No P18481-N13) and the German Research Foundation (DFG, grant No ES 70/4-1). The material investigations of the porous blankets have been made by Rieter Management AG, Winterthur, Switzerland.

References

[1] J. F. Allard. *Propagation of Sound in Porous Media*. Elsevier Applied Science, London, New York, 1993.

[2] J. F. Allard, Y. Champoux, and C. Depollier. Modelization of layered sound absorbing materials with transfer matrices. *J. Acoust. Soc. Am.*, 82(5):1792–1796, 1987.

[3] D. N. Arnold, R. S. Falk, and R. Winther. Preconditioning discrete approximations of the Reissner-Mindlin plate model. *Math. Mod. Num. Anal.*, 31(4):517–557, 1997.

[4] N. Atalla, M. A. Hamdi, and R. Panneton. Enhanced weak integral formulation for the mixed (u,p) poroelastic equations. *J. Acoust. Soc. Am.*, 109(6):3065–3068, 2001.

[5] S. Balay, J. Brown, K. Buschelman, W. D. Gropp, D. Kaushik, M. G. Knepley, L. C. McInnes, B. F. Smith, and H. Zhang. PETSc Web page, 2012. http://www.mcs.anl.gov/petsc.

[6] J. Biermann and O. v. Estorff. Beschleunigung von Multifrequenz-FE-Analysen durch die Verwendung von Gleichungsloesern mit Subspace Recycling. In *The 37th German annual conference on acoustics (DAGA)*, 2011.

[7] M. A. Biot. General theory of three-dimensional consolidation. *J. Appl. Phys.*, 12:155–164, 1941.

[8] M. A. Biot. Theory of propagation of elastic waves in a fluid-saturated porous solid.I/II. Low/Higher frequency range. *J. Acoust. Soc. Am.*, 28(2):168–191, 1956.

[9] E. de Sturler. Nested Krylov methods based on GCR. *J. Comp. Appl. Math.*, 67(1):15–41, 1996.

[10] D. Dreyer, S. Petersen, and O. v. Estorff. Effectiveness and robustness of improved infinite elements for exterior acoustics. *Comput. Methods Appl. Mech. Engrg.*, 195:3591–3607, 2006.

[11] F. Fahy. *Foundations of engineering acoustics*. Academic Press, 2001.

[12] J. Gaidamour and P. Henon. A parallel direct/iterative solver based on a Schur complement approach. In *11th IEEE International Conference on Computational Science and Engineering*, pages 98–105. Computational Science and Engineering, 2008.

[13] F. Ihlenburg. *Finite Element Analysis of Acoustic Scattering*, volume 132 of *Applied Mathematical Sciences*. Springer, Hamburg, 1998.

[14] ISO 140-3. Acoustics, measurement of sound insulation in buildings and of building elements – laboratory measurements of airborne sound insulation of building elements, 1995.

[15] Y. J. Kang and J. S. Bolton. Finite element modeling of isotropic elastic porous materials coupled with acoustical finite elements. *J. Acoust. Soc. Am.*, 98:635–643, 1995.

[16] R. Kienzler. On consistent plate theories. *Arch. Appl. Mech.*, 72:229–247, 2002.

[17] R. Kienzler. On consistent second-order plate theories. In R. Kienzler, H. Altenbach, and I. Ott, editors, *Theories of Plates and Shells: Critical Review and New Applications*, volume 16 of *Lecture Notes in Applied and Computational Mechanics*, pages 85–96. Springer-Verlag, Berlin, Heidelberg, New York, 2004.

[18] B. S. Kirk, J. W. Peterson, R. H. Stogner, and G. F. Carey. `libMesh`: A C++ Library for Parallel Adaptive Mesh Refinement/Coarsening Simulations. *Eng. Comput.*, 22(3–4): 237–254, 2006. http://dx.doi.org/10.1007/s00366-006-0049-3.

[19] L. Nagler. *Simulation of Sound Transmission through Poroelastic Plate-like Structures*, volume 10 of *Computation in Engineering and Science*. Verlag der Technischen Universität Graz, 2011.

[20] L. Nagler and M. Schanz. An extendable poroelastic plate formulation in dynamics. *Arch. Appl. Mech.*, 80:1177–1195, 2010.

[21] M. L. Parks, E. de Sturler, G. Mackey, D. D. Johnson, and S. Maiti. Recycling Krylov subspaces for sequences of linear systems. *SIAM J. Sci. Comput.*, 28(5):1651–1674, 2006.

[22] P. Rong, O. v. Estorff, L. Nagler, and M. Schanz. An acoustical finite shell element for the simulation of air layers. *J. Comp. Acoustics*, page (accepted), 2013.

[23] Y. Saad and B. Suchomel. Arms: An algebraic recursive multilevel solver for general sparse linear systems. *Num. Lin. Alg. Appl.*, 9:359–378, 2002.

[24] M. Wandel. *Validation of A400M FE-Model for Primary Insulation and Lining Material*. Technischer Bericht, Airbus-Akustikabteilung, Hamburg, 2006.

[25] O.C. Zienkiewicz and R.L. Taylor. *The Finite Element Method*. Butterworth Heinemann, 5 edition, 2000.